C. R. Mecanique 341 (2013) 35–43

Contents lists available at SciVerse ScienceDirect

Comptes Rendus Mecanique

www.sciencedirect.com

Combustion, flow and spray dynamics for aerospace propulsion

Flapping instability of a liquid jet

Instabilité de flapping d'un jet liquide

Jean-Philippe Matas *, Alain Cartellier

LEGI–CNRS–université de Grenoble, BP 53, 38041 Grenoble cedex 9, France

ARTICLE INFO

Article history:
Available online 3 January 2013

Keywords:
Instability
Drop formation
Atomization

Mots-clés :
Instabilité
Formation de gouttes
Atomisation

ABSTRACT

We study the flapping instability observed when a liquid jet is incompletely atomized by a fast parallel gas stream: the remaining liquid jet is destabilized over a scale large compared with its radius, and breaks into liquid fragments. We characterize the symmetry of this instability and its frequency. The intact liquid length is measured as a function of gas and liquid velocity, and turns out to be longer than the one predicted by Raynal (1997) for a planar mixing layer. The frequency of the instability is measured with a spectral method, and is in agreement with the frequency observed for the planar shear instability, though slightly smaller. The planar, and not helical, symmetry of the instability makes it akin to a flapping instability, observed when a planar liquid sheet is atomized by two planar gas streams. We next measure drop sizes when the flapping instability is present, with a method based on image processing. Measured size distributions are in agreement with distributions observed in a mixing layer geometry for low gas velocities (long tail distribution). The mean drop diameter depends weakly on liquid velocity, and decreases as $d_{10} \sim U_g^{0.9}$. On the contrary, Sauter diameter depends strongly on liquid velocity.

RÉSUMÉ

Nous étudions l'instabilité de flapping observée lors de l'atomisation incomplète d'un jet liquide par un cocourant gaz : le jet liquide non atomisé se déstabilise sur une échelle grande par rapport à son rayon, et se brise en fragments liquides. Nous caractérisons dans un premier temps cette instabilité en mesurant sa fréquence, sa symétrie, et la répartition spatiale du liquide qu'elle entraîne. La longueur du cône liquide est mesurée en fonction des vitesses gaz et liquide, et s'avère significativement plus longue que celle prédite par Raynal (1997) pour une couche de mélange plane. La fréquence de l'instabilité est mesurée par une méthode spectrale, et s'avère proche de celle observée pour l'instabilité de cisaillement, mais légèrement inférieure. L'instabilité a une symétrie plane, et non hélicoïdale, et semble ainsi s'apparenter au flapping d'une nappe liquide atomisée par deux nappes parallèles gaz. Le plan de l'instabilité est par contre orienté de façon aléatoire. Nous proposons un scénario pour le mécanisme de cette instabilité, en nous basant sur l'instabilité des modes non axisymétriques de l'instabilité de cisaillement. Nous caractérisons ensuite les tailles de gouttes produites lorsque l'instabilité de flapping est présente, par visualisation et traitement d'image : les distributions de tailles de gouttes mesurées se rapprochent des distributions observées en atomisation plane pour des conditions de faible vitesse gaz (décroissance lente aux grandes tailles de gouttes). Le diamètre moyen des gouttes ne dépend que faiblement de la vitesse du jet liquide, et

* Corresponding author.
E-mail address: jean-philippe.matas@hmg.inpg.fr (J.-P. Matas).

1631-0721/$ – see front matter
http://dx.doi.org/10.1016/j.crme.2012.10.006

décroit en $d_{10} \sim U_g^{0,9}$. Le diamètre de sauter dépend par contre fortement de la vitesse liquide.

1. Introduction

Assisted atomization of a liquid jet, also known as airblast atomization, is fundamental to many applications. In this process liquid is stripped from a cylindrical jet by a fast co-current air stream, and a spray is produced [1,2]. Applications range from injectors in turboreactors, to cryotechnic rocket engines with LOX/H2. This process is widely used, and has proven reliable, but the mechanism by which the liquid bulk is broken into droplets is still subject to controversy. A better understanding of the different stages of the atomization process could help improve the efficiency of combustion, and decrease the amount of emissions.

Experiments carried out on a planar mixing layer [3] and on a coaxial injector [4] have shown that the liquid break up is the result of two successive instabilities. The first instability is a shear instability, analogous to a Kelvin–Helmholtz instability but controlled by the thickness of the gas vorticity layer δ_g, and leads to the formation of 2D longitudinal waves at the interface between the liquid and the fast gas stream. An inviscid stability analysis, based on a realistic velocity profile including a velocity deficit at the interface, predicts the following most unstable mode wavenumber and corresponding frequency [3]:

$$k = \sqrt{r}/\delta_g\left(\sqrt{2} + \frac{3}{2}M^{-1/2}\right) \quad \text{and} \quad \omega_r = r\frac{U_g}{\delta_g}\left(1 + \frac{5}{2}\sqrt{2}M^{-1/2}\right)$$

where $r = \rho_g/\rho_l$ is the gas to liquid density ratio, U_g and U_l are the respective gas and liquid velocities, and where M stands for the dynamic pressure ratio $M = \rho_g U_g^2/(\rho_l U_l^2)$. Agreement between this prediction and the frequency measured in a planar geometry is good [3]. In a coaxial geometry, the same mechanisms holds and the corresponding waves exhibit an axisymmetric geometry: in the latter geometry though, experimental frequencies are significantly larger than predicted ones [4], a point which is still the subject of investigation.

The waves resulting from this instability are next accelerated by the fast gas stream, and undergo a Rayleigh–Taylor transverse instability, leading to the formation of liquid ligaments [4,5]. These ligaments grow and eventually break into droplets, whose size is controlled by the thickness of ligaments, and hence the wavelength of the R–T instability.

When the liquid intact length is larger than the potential cone, atomization of the liquid jet is incomplete: while small droplets are still produced in the potential cone region, far downstream the liquid jet ends up breaking into large liquid lumps. Just before its break-up, the liquid jet downstream the potential cone exhibits a striking “oscillating” aspect, in which it undergoes oscillations of a wavelength large compared to the jet diameter (see Fig. 1). Our study is devoted to this large scale instability, called here the “flapping” instability.

2. Experimental set-up

A round vertical liquid jet is entrained by a fast coaxial annular gas stream (Fig. 2). Injection is made through smooth convergent nozzles. The contraction factor is 6.9 for the liquid jet (exit diameter 8 mm), and 6 for the gas jet (outer exit diameter 11.4 mm). The convergence in the injector ensures that the intensity of perturbations is reduced. The liquid is water. Gas flow is measured with a mass flowmeter (Brooks Instruments), and liquid flow is measured with a rotameter (Kobold).

The liquid velocity U_l was varied in the range [0.11 m/s, 1 m/s], and the gas velocity U_g in the range [15 m/s, 60 m/s]. For these ranges of velocities and the smooth convergent injector we used, the flow is laminar in the liquid and gas boundary layers. The three dimensional structure of the flow was captured with a single camera and a vertical mirror placed at 45 degrees next to the nozzle (see Fig. 2): this device allows to capture on a same frame the front view and side view of the atomized jet, and consequently the three dimensional geometry of the flow. The camera is a high speed camera (Phantom v12), and frames are taken for a frequency in the range [500 im/s; 2000 im/s] depending on the gas velocity.

3. Experimental results and discussion

Fig. 3 shows how the liquid jet is atomized for gas and liquid velocities of $U_g = 40$ m/s and $U_l = 0.3$ m/s respectively. For this regime, a large number of small drops are produced near the injection, when liquid is stripped from the bulk of the jet by the fast air stream. However, it can be seen in Fig. 3 that large liquid fragments remain intact on the axis of the jet: though the jet undergoes a strong destabilization, these fragments cause the formation of large drops far downstream. This destabilization of the bulk of the jet is due to the flapping instability studied in this work. When the gas velocity is decreased, the growth rate of both the shear and Rayleigh–Taylor instabilities is strongly reduced and the flapping instability becomes the dominant mechanism in the break-up of the jet: liquid is not stripped from the jet anymore, as in Fig. 1. This instability of relatively large wavelength leads the jet to twist and break into fragments of typical size R. The

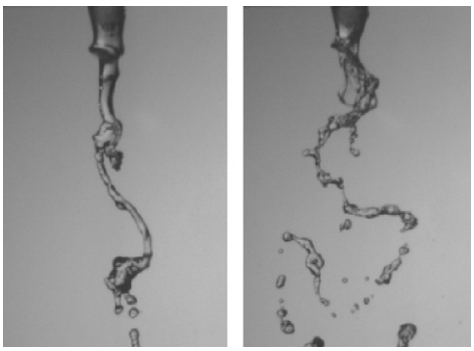

Fig. 1. Instability of a liquid jet in airblast atomization for: (a) $U_g = 25$ m/s and $U_l = 0.15$ m/s; (b) $U_g = 30$ m/s and $U_l = 0.15$ m/s.

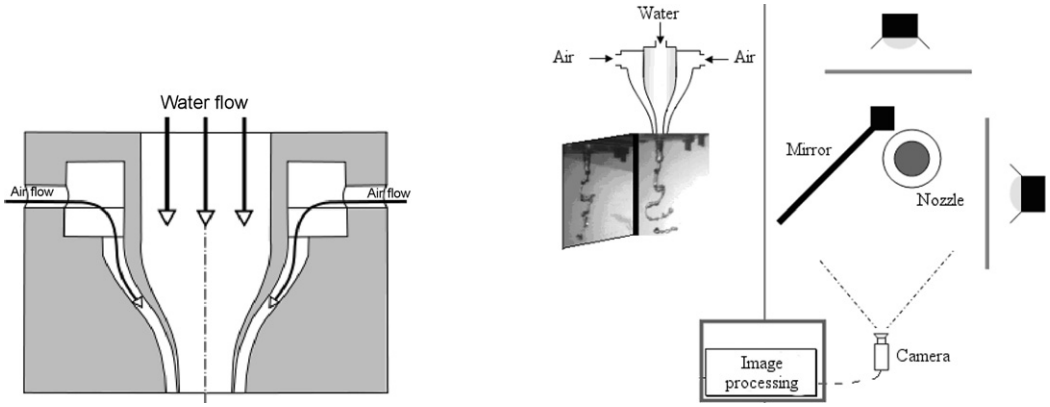

Fig. 2. Left: Sketch of the nozzle used in the experiment. Right: Front view and top view of the experimental set-up.

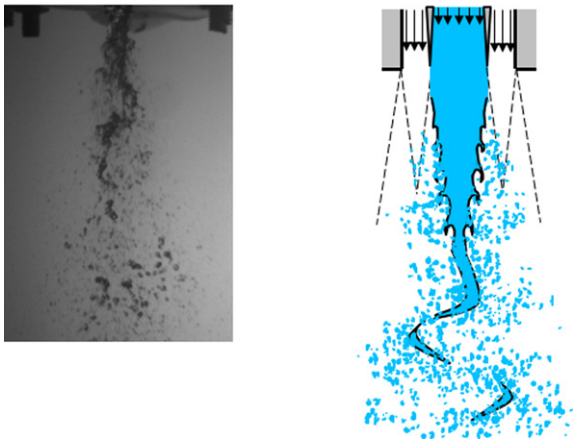

Fig. 3. Left: Airblast atomization for $U_g = 40$ m/s and $U_l = 0.3$ m/s. Right: sketch emphasizing how the flapping instability creates large liquid fragments.

flapping instability is therefore especially relevant in situations when Kelvin–Helmholtz and Rayleigh–Taylor instabilities fail to completely atomize the jet: this occurs in particular when the length of the gas potential cone (shown by dashed line in the sketch of Fig. 3) is shorter than the liquid intact length. In our experiment this is generally true. This means that the ultimate break-up of the jet is likely to be controlled by the flapping instability.

In order to measure the intact length of the liquid jet, images taken with the device shown in Fig. 2 are processed according to the following sequence: the images are thresholded, we use a Matlab routine to find all paths on the image,

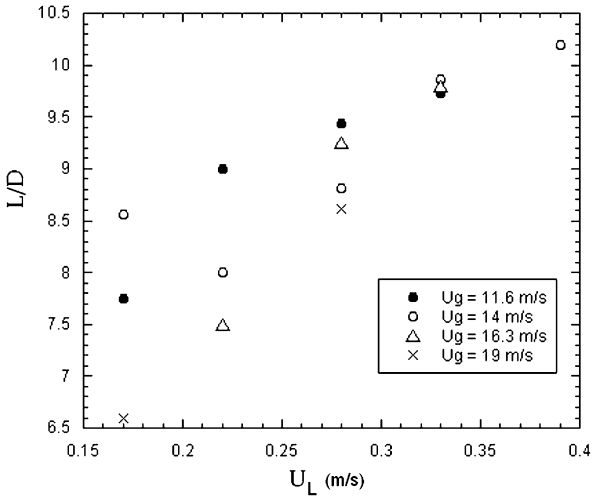

Fig. 4. Liquid intact length L of the jet, nondimensionalized by the liquid injector diameter D, as a function of liquid velocity U_l, for different gas velocities U_g.

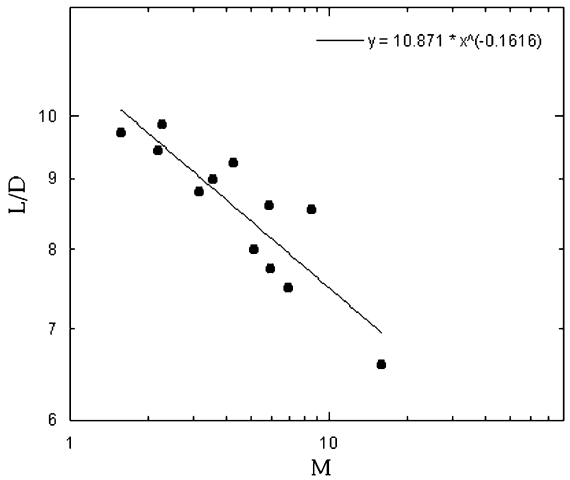

Fig. 5. Logarithmic plot of the ratio L/D as a function of M. The exponent of the power law fit indicates a much slower decrease than the $M^{-1/2}$ scaling predicted by Raynal [6].

and the jet is taken to be the longer path on each image. The intact length is taken to be the distance between the injector and the point belonging to the longest path which is farthest from the injector. The intact length for a given set of gas and liquid velocity is averaged over 300 images. This process is only carried out for the front images of the jet (the mirror images are not used for this measurement). The intact length L is then nondimensionalized by the liquid jet diameter D, results are shown in Fig. 4. The data of Fig. 4 show that as expected the liquid intact length decreases with increasing gas velocity U_g, and increases with increasing liquid velocity U_l. These measurements were only carried out for conditions where the flapping instability was present, i.e. the liquid jet exhibits large scale oscillations. Raynal (1997) proposed a scaling for the liquid intact length [6]: $L/D \approx 6/\sqrt{M}$. This scaling has been verified experimentally on his plane shear layer experiment (liquid sheet flowing on a solid wall and atomized by a parallel fast gas stream).

In Fig. 5 we plot the ratio L/D as a function of M: it can be seen that though M appears to be a relevant parameter (the data of Fig. 4 are indeed collapsed), the scaling law observed experimentally is quite different from the one predicted by Raynal [6]. The decrease of L/D with M is much slower, and the values of L/D are significantly larger (longer relative intact length). This could be due to the fact that for our conditions the liquid intact length is set not only by the amount of fluid stripped by the gas from the jet (as argued by Raynal [6]), but also by the amplitude of the flapping instability. As mentioned above, this is mainly because the liquid intact length largely exceeds the length of the potential cone. We next show measurements of the angle of aperture of the jet: these measurements are taken by superposing all images obtained for a given set of conditions. Fig. 6a shows a typical result for this operation, for a liquid velocity $U_l = 0.28$ m/s and a gas velocity $U_g = 14$ m/s. The resulting image shows that there is a constant angle over a relatively large downstream distance. The angle is measured in the region close to the injector, where the edges of the superposition are cleaner. We plot the

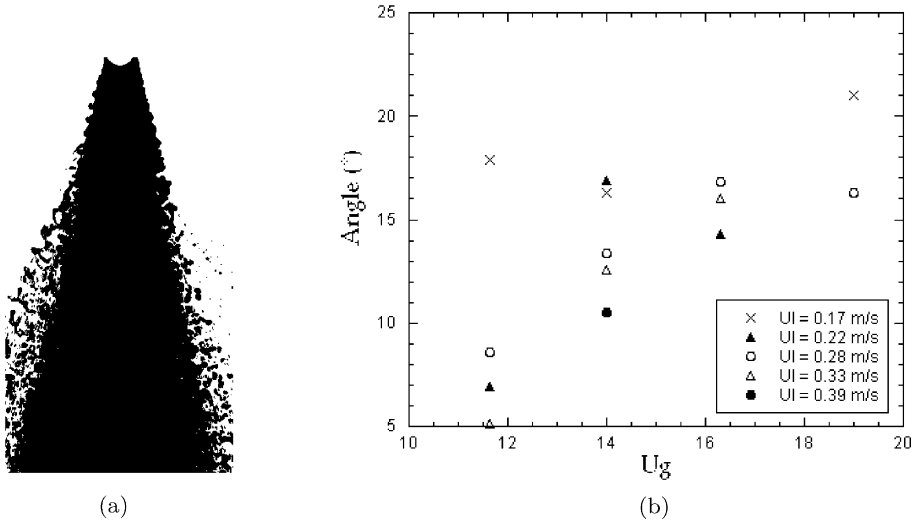

Fig. 6. (a) Superposition of the successive positions of the jet, for $U_g = 14$ m/s and $U_l = 0.28$ m/s. (b) Angle of aperture of the jet as a function of gas velocity, for different liquid velocities.

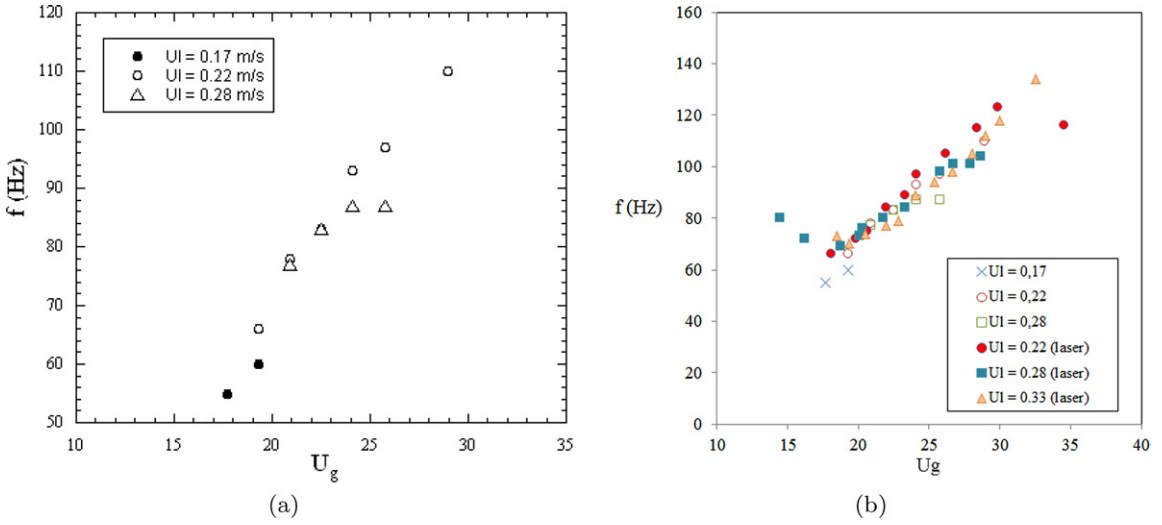

Fig. 7. Frequency of the flapping instability as a function of gas velocity, for different liquid velocities. (a) Frequency is measured via image processing. (b) Same data, with additional points measured with laser–photodiode apparatus.

measured angle when gas and liquid velocities are varied in Fig. 6b. As expected, the angle increases with the gas velocity and decreases with increasing liquid velocity, i.e. when the momentum of the liquid is increased. The measurements for the lowest liquid velocity ($U_l = 0.17$ m/s, represented by crosses in Fig. 6b) exhibit significantly larger angles than for larger liquid velocities: this could be due to the fact that for this very low liquid velocity the jet thins extremely quickly downstream the injector due to its acceleration, and probably undergoes Rayleigh–Plateau break-up.

Measurement of the wavelength of the instability has been attempted, but results are inconclusive due to the strong spatial variation of the wavelength as a function of the downstream distance: this is evidenced in Fig. 1b for example, where it can be seen that the first wavelength is significantly smaller than the second one (presumably due to the increase in velocity of the liquid). We therefore choose to focus instead on the frequency of the instability.

The main difficulty for this measurement is that the flapping instability occurs roughly within a same plane, but a plane of changing orientation. The orientation of the plane of oscillation changes after a few periods, and appears to be random. Two methods were tested for the frequency measurement. The first method relies on image processing. In order to get rid of the tridimensionality of the instability, the images taken with the apparatus shown in Fig. 2 are processed according to the following procedure:

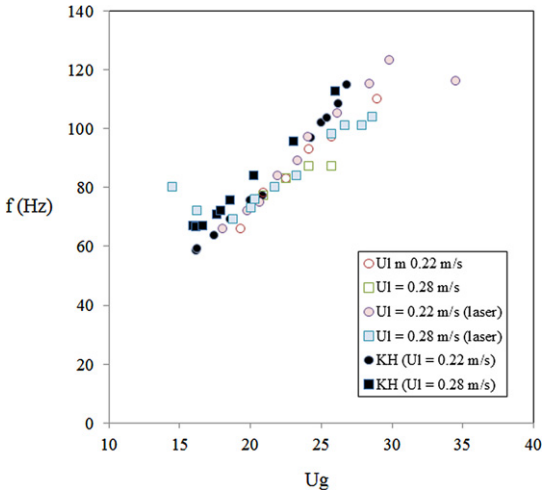

Fig. 8. Frequency of the flapping instability and of the Kelvin–Helmholtz instability (black symbols) as a function of gas velocity U_g, for two liquid velocities.

- Images are thresholded, and only the dark region connected to the injector is retained (drops and detached ligaments are therefore removed).
- The center of this region for a given height is computed on the mirror image (this is position x) and on the front image (position y): the distance of the jet center from the axis of the injector is then defined as $r = (x^2 + y^2)^{1/2}$.
- The variations of $r(t)$ are computed for several heights (distances from the injector), and a Fourier transform of this signal directly yields the frequency of the oscillation.

We find that the maximum frequency is independent of the distance from the injector, provided that the measurement is made far enough from the injector. Measurements close to the injector might be affected by the Kelvin–Helmholtz instability: the latter instability is expected to produce axisymmetric waves close to the injector, but any alteration to the symmetry of the waves could induce a variation of the distance r (distance of the jet center from the axis) at the KH frequency. This is why we take care to measure the frequency of the flapping instability farther downstream, in regions where the flapping is visually predominant (criterion: the axis of the jet is displaced from the axis of the injector of a distance larger than R). The frequency of the flapping instability measured with this system is shown in Fig. 7a as a function of gas velocity, for three different liquid velocities. It increases with gas velocity. Only points where a maximum frequency was clearly apparent in the spectrum were kept for the results of Fig. 7a. In order to be able to measure the frequency of the flapping instability for a larger range of conditions, we also used a simpler laser–photodiode method: a laser beam is aimed at the jet, and a photodiode set opposite the liquid jet measures the intensity of the laser after it is refracted by the liquid. The signal is then Fourier transformed, as in the first method, and the maximum frequency is retained. Contrary to the first method, this measurement cannot ensure that the measured frequency is associated with a flapping instability: the measured frequency could result from an axisymmetric instability similar to the KH instability observed close to the injector. However, care is taken to carry out the measurement far downstream the injection (about ten nozzle diameters downstream), in a region where the flapping distorts strongly the liquid jet. The frequencies measured with this method are shown on Fig. 7b. They are in good agreement with the frequencies measured with the other method.

We can compare these data points with the measurements of the Kelvin–Helmholtz instability carried out in a previous experiment (see Fig. 8). The KH instability was measured by the aforementioned laser–photodiode method, but with both the laser and the photodiode located just below the injector, and the laser beam aimed at the edge of the jet instead of its center: the signal is periodically interrupted by the KH waves, and the frequency can be measured precisely up to much larger velocities than with image processing methods. It can be seen in Fig. 8 that the frequency of the KH instability is slightly larger than the flapping instability, but that both frequencies are relatively close. We emphasize that both instabilities were measured at different locations: very close to the injector for the KH instability, and far downstream for the flapping: measurements of both series were made as independent as possible, and the closeness of the results is probably a clue to the physical link between both instabilities in our experimental conditions.

Though the range of gas velocity U_g is not large enough to predict a scaling of the flapping frequency with gas velocity, the experimental points of Fig. 7 are consistent with a frequency proportional to U_g. This is the scaling law experimentally measured by Lozano et al. [7] on their liquid sheet experiment (a rectangular liquid sheet atomized by two parallel gas streams). This is also the scaling found by Couderc (2007) in his numerical simulation of the same liquid sheet configuration [8]. The analogy between their configuration and ours resides in the limit of the jet instability when the radius is decreased: for a large radius KH instability is merely a surface instability, but when R becomes of the order of magnitude of the KH instability wavelength, sinuous modes analogous to the flapping modes of a liquid sheet may start to overcome the axisymmetric instability. For a flapping sheet it is known [9] that the sinuous mode overcomes the varicose mode: it is

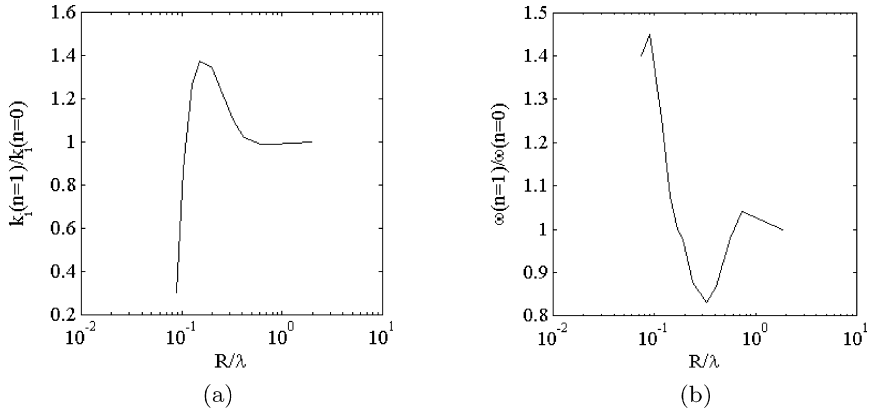

Fig. 9. Result of the inviscid stability analysis in cylindrical geometry: (a) Ratio of the growth rates of the unstable helical mode and axisymmetric mode as a function of the ratio R/δ. (b) Frequency ratio for the same modes.

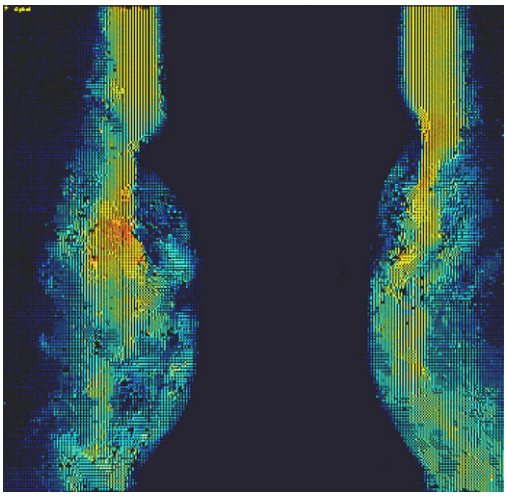

Fig. 10. PIV visualization of the gas velocity field around the liquid jet: the flow is nonaxisymmetric. $U_g = 10$ m/s and $U_l = 0.4$ m/s.

relatively easier for waves on opposing sides to propagate with opposing phases (sinuous mode) than with the same phase (varicose mode).

In our configuration this has been verified by solving the inviscid linear stability analysis in axisymmetric geometry for helical modes of the form $e^{i(kx-\omega t+n\theta)}$ with $n \neq 0$. The resulting dispersion relation is solved for spatial modes, i.e. complex wavenumber k and real frequency ω. We find in particular that the $n = 1$ mode is unstable. The focus of this article being on the experimental study of the flapping instability, we just present in Fig. 9a the ratio of the resulting growth rate for the axisymmetric mode ($n = 0$) and the helical mode ($n = 1$): it can be seen that when the radius of the jet is decreased, the growth rate of the helical mode overcomes that of the varicose mode. Note that in Fig. 9, R is nondimensionalized by the wavelength λ of the $n = 0$ mode. In our experimental conditions $R/\lambda \sim 0.3$ (the ratio increases when the gas velocity is increased), which falls in the region where the helical mode is significantly more unstable than the $n = 0$ mode (see Fig. 9a). Fig. 9b shows the frequency ratio for the same modes: interestingly the frequency of the helical mode $n = 1$ is slightly smaller than the frequency of the axisymmetric mode for the conditions of our experiment.

This might be at the origin of, or at least enhance, the flapping instability: Fig. 10 shows a PIV visualization of the gas velocity field around the liquid jet for experimental conditions for which the flapping instability is observed farther downstream. The PIV is carried out with a laser slice of the coaxial jet, and a seeding of the gas phase with oil droplets. Fig. 10 shows how the gas jet detaches from the liquid jet downstream the first KH wave, causing large gas recirculations scaling with the KH wavelength. In particular, it can be noticed how the slight dissymmetry in the KH wave (the left side of the wave is a bit ahead the right side) induces a dissymmetry in the way the gas jet impacts the liquid jet downstream the large recirculations: we suspect this is the mechanism responsible for the flapping instability.

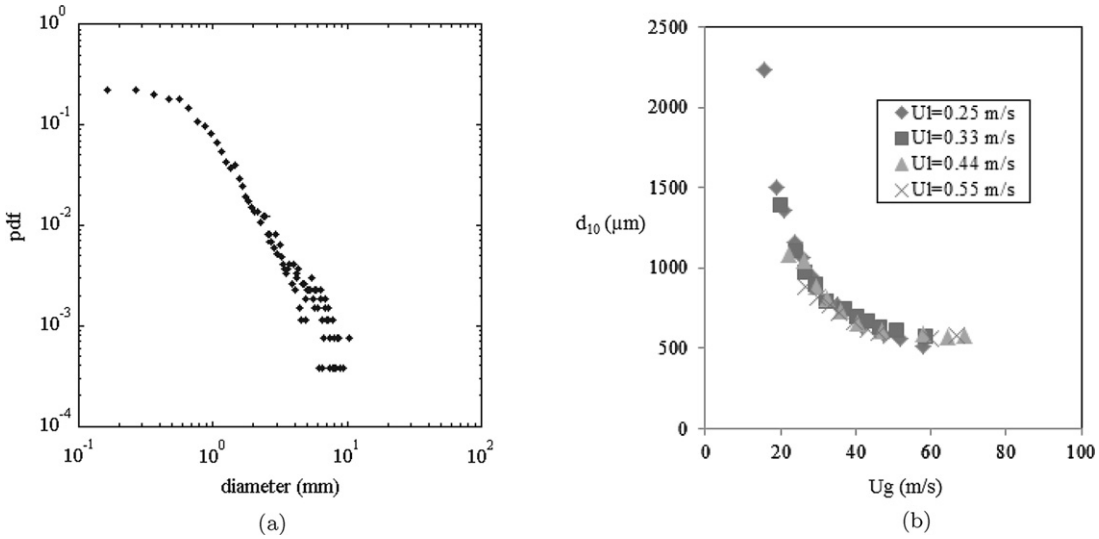

Fig. 11. (a) Histogram of drop mean diameters for $U_l = 0.33$ m/s and $U_g = 23$ m/s. (b) Variations of the drop mean diameter as a function of U_g, for different values of U_l.

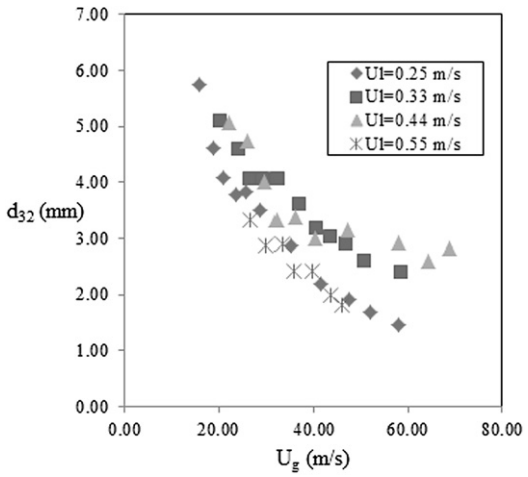

Fig. 12. Variations of the Sauter diameter d_{32} as a function of U_g, for different liquid velocities.

4. Drop size measurements

We now present drop size measurements, for regimes where the flapping instability is present. Drop size is measured via image processing: images are taken of a square region located between 10 and 20 liquid diameters downstream the injection. This region is thresholded, drops touching the edges of the region are removed, and drops whose surface is smaller than 8 pixels are removed. This limit of 8 pixels squared corresponds to a minimum size of 100 μm below which drop size was observed to be poorly reliable. A program then computes the location of all remaining droplet sizes and centers on the image. A droplet is therefore defined as an isolated liquid region detached from the edges of the image. Fig. 11a shows a typical size distribution obtained by this method. The method has a poor resolution for low sizes (the cut-off size is 100 μm), however the distribution is well captured for large sizes, and exhibits a relatively slow exponential decrease. This decrease is consistent with the one observed with another method (optical probe) on a planar mixing layer experiment, where the atomization mechanism is presumed to be the same except for the flapping instability [10].

Fig. 11b shows the variation of the first moment of this distribution, mean diameter d_{10}, as a function of gas velocity U_g, for different values of U_l. The mean drop size decreases rapidly when U_g is increased, but does not appear to depend on liquid velocity. Fig. 12 shows the variations of the Sauter mean diameter d_{32} (SMD) as a function of U_g, for different liquid velocities: though d_{32} decreases consistently with U_g, it can be seen on this graph that liquid velocity also has an impact. SMD increases when liquid velocity is increased from 0.25 m/s to 0.44 m/s. This is consistent with the decrease in M related to this increase: for a given gas velocity, the liquid will resist more to the stripping for larger U_l. However, for the series investigated at the largest liquid velocity, $U_l = 0.55$ m/s, SMD undergoes a steep decrease, and is almost smaller than

for $U_g = 0.25$ m/s, a liquid velocity twice as small. We think this apparently surprising result is related to the vanishing of the flapping instability: for $U_l = 0.55$ m/s and the gas velocities investigated here, the flapping instability has a very small amplitude, and is not capable anymore of creating large drops.

5. Conclusion

We have studied the flapping instability of a liquid jet, an instability occurring downstream the Kelvin–Helmholtz shear instability when the liquid jet has not been fully atomized. We have presented measurements of the frequency of this instability, which is close to, but smaller than the frequency of the KH instability. We offer a scenario for the development of the instability, based on the dissymmetry induced in the gas flow when nonaxisymmetric modes overcome the varicose modes. Further experiments need be carried out for different conditions (in particular different radii of the liquid jet, different thicknesses of the gas stream) in order to investigate more precisely this hypothesis, and to precise the scaling of the flapping frequency.

Measurements of drop sizes produced in presence of this instability were carried out with an image processing method. We observed that the mean diameter is not influenced by the liquid velocity, while Sauter diameter is. While size distributions are consistent with typical exponential distributions obtained on a planar set-up where there is no flapping behavior, the flapping instability may explain the nonmonotonous behavior of d_{32} when liquid velocity is increased.

Acknowledgements

We acknowledge discussions with Jean-Luc Estivalezes, in particular regarding the related flapping sheet configuration. This work has been supported by the French National Agency (ANR), project VAA.

References

[1] J. Lasheras, E.J. Hopfinger, Liquid jet instability and atomization in a coaxial gas stream, Annu. Rev. Fluid Mech. 32 (2000) 275–308.
[2] J. Eggers, E. Villermaux, Physics of liquid jets, Rep. Prog. Phys. 71 (2008) 036601.
[3] J.-P. Matas, S. Marty, A. Cartellier, Experimental and analytical study of the shear instability of a gas–liquid mixing layer, Phys. Fluids 23 (2011) 094112.
[4] P. Marmottant, E. Villermaux, On spray formation, J. Fluid Mech. 498 (2004) 73.
[5] M. Hong, A. Cartellier, E.J. Hopfinger, Atomization and mixing in coaxial injection, in: Proc. 4th Int. Conf. on Launcher Technology, Liège, Belgium, 2002.
[6] L. Raynal, Instabilité et entraînement à l'interface d'une couche de mélange liquide–gaz, PhD thesis, Université J. Fourier Grenoble I, France, 1997.
[7] A. Lozano, F. Barreras, C. Siegler, D. Löw, The effects of sheet thickness on the oscillation of an air-blasted liquid sheet, Exp. Fluids 39 (2005) 127–139.
[8] F. Couderc, Développement d'un code de calcul pour la simulation d'écoulements de fluides non miscibles. Application à la désintégration assistée d'un jet liquide par un courant gazeux, PhD thesis, ENSAE Toulouse, France, 2007.
[9] S.P. Lin, Breakup of Liquid Sheets and Jets, Cambridge University Press, 2003.
[10] S. Marty, J.-P. Matas, A. Cartellier, Study of a liquid–gas mixing layer: Shear instability and size of produced drops, in: 3rd INCA Colloquium, Onera-Toulouse, 17–18 November 2011.